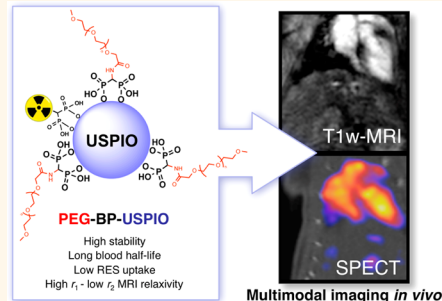


Bisphosphonate-Anchored PEGylation and Radiolabeling of Superparamagnetic Iron Oxide: Long-Circulating Nanoparticles for *in Vivo* Multimodal (T1 MRI-SPECT) Imaging

Lydia Sandiford,[†] Alkystis Phinikaridou,[†] Andrea Protti,[†] Levente K. Meszaros,[†] Xianjin Cui,[†] Yong Yan,[‡] George Frodsham,[§] Peter A. Williamson,[†] Nicholas Gaddum,[†] René M. Botnar,[†] Philip J. Blower,^{†,✉} Mark A. Green,^{†,*} and Rafael T. M. de Rosales^{†,*}

[†]Division of Imaging Sciences and Biomedical Engineering, King's College London, St. Thomas' Hospital, London, SE1 7EH, U.K., [‡]School of Chemistry, University of Nottingham, University Park, Nottingham, NG7 2RD, U.K., [§]The Davy Faraday Research Laboratory, The Royal Institution of Great Britain, 21 Albemarle Street, London, W1S 4BS, U.K., and [✉]Department of Chemistry, King's College London, Hodgkin Building, Guy's Campus, London, SE1 1UL, U.K.

ABSTRACT The efficient delivery of nanomaterials to specific targets for *in vivo* biomedical imaging is hindered by rapid sequestration by the reticuloendothelial system (RES) and consequent short circulation times. To overcome these two problems, we have prepared a new stealth PEG polymer conjugate containing a terminal 1,1-bisphosphonate (BP) group for strong and stable binding to the surface of ultrasmall-superparamagnetic oxide nanoparticles (USPIOs). This polymer, PEG(5)-BP, can be used to exchange the hydrophobic surfactants commonly used in the synthesis of USPIOs very efficiently and at room temperature using a simple method in 1 h. The resulting nanoparticles, PEG(5)-BP-USPIOs are stable in water or saline for at least 7 months and display a near-zero ζ -potential at neutral pH. The longitudinal (r_1) and transverse (r_2) relaxivities were measured at a clinically relevant magnetic field (3 T), revealing a high r_1 of $9.5 \text{ mM}^{-1} \text{ s}^{-1}$ and low r_2/r_1 ratio of 2.97, making these USPIOs attractive as T1-weighted MRI contrast agents at high magnetic fields. The strong T1-effect was demonstrated *in vivo*, revealing that PEG(5)-BP-USPIOs remain in the bloodstream and enhance its signal 6-fold, allowing the visualization of blood vessels and vascular organs with high spatial definition. Furthermore, the optimal relaxivity properties allow us to inject a dose 4 times lower than with other USPIOs. PEG(5)-BP-USPIOs can also be labeled using a radiolabeled-BP for visualization with single photon emission computed tomography (SPECT), and thus affording dual-modality contrast. The SPECT studies confirmed low RES uptake and long blood circulation times ($t_{1/2} = 2.97 \text{ h}$). These results demonstrate the potential of PEG(5)-BP-USPIOs for the development of targeted multimodal imaging agents for molecular imaging.



KEYWORDS: bisphosphonates · superparamagnetic iron oxide · PEG · RES · USPIO · MRI · SPECT · multimodal imaging

The use of nanoparticle (NP) technologies for biomedical purposes such as imaging or drug delivery is an area of major interest. In the field of imaging, NPs offer several properties that make them particularly attractive.^{1–3} For example, NPs can be designed to contain multiple copies of functional groups such as chelators and targeting ligands and hence provide high imaging signal strength and target avidity. In addition their surfaces can be exploited to control their colloidal properties. However, the use of NPs for *in vivo* imaging has some

drawbacks. For example, unlike small molecules and peptides, the size of most NPs prevents passive diffusion through normal endothelium. Perhaps the major disadvantage is that most NPs are quickly recognized and sequestered by circulating macrophages and Kupffer cells of the reticuloendothelial system (RES) present in the liver and spleen. In addition, NPs are prone to the formation of aggregates with large diameters (several micrometers) that can be irreversibly trapped in the capillaries of the lungs. These two effects not only represent

* Address correspondence to rafael.torres@kcl.ac.uk.

Received for review October 4, 2012 and accepted November 29, 2012.

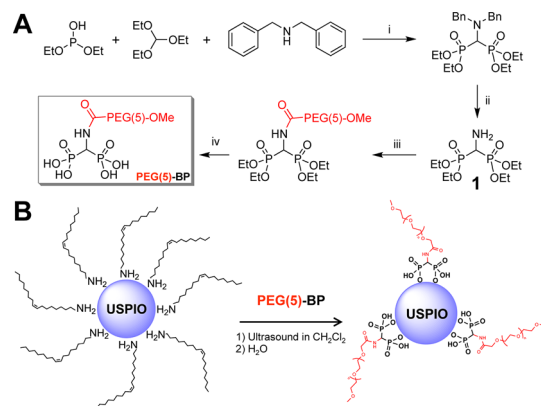
Published online November 29, 2012
10.1021/nn3046055

© 2012 American Chemical Society

a potential toxicity threat for the subject but also result in short circulation times and failure to reach the intended target. Thus, in order to develop effective NPs for *in vivo* imaging of molecular targets, there is a need to minimize RES uptake, avoid *in vivo* aggregation and prolong circulation times. Furthermore, NPs need to be nontoxic, or to be excreted as fast as possible after the procedure.

The most successful nanoparticle platform for *in vivo* imaging to date has been based on iron oxide materials, and in particular superparamagnetic iron oxide NPs (SPIOs).^{4–9} This success is not only due to their properties as magnetic resonance imaging (MRI) contrast agents but also due to their low toxicity as proven by more than 20 years of clinical use. Most iron oxide nanomaterials are quickly recognized by the macrophages of the RES, making them useful as contrast agents for tissues of the liver and spleen, or by macrophages present in inflamed tissues. The SPIOs are decomposed inside these cells and the iron is assimilated by the body for the synthesis of essential metalloproteins such as hemoglobin.¹⁰ For many targeted imaging applications, as discussed above, it is desirable to extend their circulation time, avoid aggregation, and minimize RES uptake. A well-established strategy to extend the circulation times of these particles is to use ultrasmall SPIOs (USPIOs). These smaller NPs (<50 nm diameter) have shown longer blood half-lives compared to their bigger counterparts, making them useful for angiographic imaging using T1-weighted MR imaging. Nevertheless they still show high levels of RES uptake.⁸ Two main factors control the RES uptake of NPs: opsonization and aggregation/size. Opsonization is a process by which xenobiotic materials are tagged with opsonin proteins to initiate association with circulating/stationary macrophages. Aggregation is a problem because RES uptake increases with NP size, regardless of the surface properties. To control both of these processes, the properties of the NP surface are critical.^{11,12}

The most successful strategy to minimize opsonization and aggregation, and hence RES uptake, is to coat the NP surface with hydrophilic polymers such as polyethylene glycol (PEG).¹¹ This biocompatible polymer works by providing (1) a hydrophilic layer that makes the NPs dispersible in water, and (2) inter-NP steric repulsion to prevent aggregation. Here, we present a simple method of surface PEGylation for USPIOs that relies on the high affinity of 1,1-bisphosphonates (BPs) toward metal oxide materials. Recently, using radiolabeled BPs, we were able to measure that BPs bind very strongly to several metal oxides, including clinically approved SPIOs that get taken by the RES, providing a useful method to radiolabel these materials.^{13,14} In this work, we aimed at fully exploiting BP anchors to synthesize a long-circulating USPIO for MR angiography. To this end, we synthesized a PEG-BP



Scheme 1. (A) Synthesis of PEG(5)-BP. Reaction conditions: (i) 29 h at 150–160 °C under N_2 ; (ii) 48 h, H_2 , 10% Pd/C, EtOH, RT; (iii) MeO-PEG(5)-COOH (1 equiv), DCC, CH_2Cl_2 , 20 °C; (iv) 48 h, TMBS (15 equiv), CH_2Cl_2 , RT then 1.5 h in MeOH. (B) Synthesis of PEG(5)-BP-USPIO.

conjugate and evaluated its use to coat USPIOs and produce hydrophilic NPs with high stability *in vivo* and optimal properties as a T1 MRI contrast agent. In addition, we aimed to use radiolabeled BP conjugates for use with nuclear imaging techniques such as single photon emission computed tomography (SPECT) and positron emission tomography (PET) and thus affording dual-modality contrast.

RESULTS AND DISCUSSION

Synthesis of PEG(5)-BP. The reaction scheme for the synthesis of PEG(5)-BP is shown in Scheme 1A. Tetraethyl aminomethyl-bisphosphonate (**1**), was synthesized following published methods.^{15,16} Briefly, a mixture of diethyl phosphite, triethylorthoformate and dibenzylamine were reacted for 29 h at 150–160 °C to give the benzylated bisphosphonate, followed by debenzylation with H_2 and 10% Pd/C catalyst. After removal of the catalyst, **1** was reacted for 16 h with MeO-PEG-COOH (5 kDa) using dicyclohexylcarbodiimide (DCC) activation. The formation of a substantial amount of insoluble white needles that we believe to be dicyclohexylurea suggested the progress of the reaction. This precipitate was removed by three cycles of filtration—concentration of the reaction solution. Once all the precipitate had been removed, the product was dried, dissolved in anhydrous dichloromethane, and reacted with 15 equiv of trimethylsilyl bromide (TMBS) for two days at room temperature (RT) to deprotect the phosphonate groups. The volatile products were then removed and the residue was stirred in HPLC-grade methanol for 1.5 h, dried, dissolved in water, and dialyzed overnight using a dialysis membrane with a molecular weight cutoff of 3500 Da to remove any small molecules present. The product, PEG(5)-BP, was obtained as a white powder and characterized using ^{31}P NMR and infrared (IR) spectroscopy. The IR spectrum shows no clear differences between PEG(5)-COOH and PEG(5)-BP, due to the small changes

and substantial overlap of the $-\text{CH}_2-$ and $-\text{PO}_3$ vibrations. There are two changes in the spectrum that confirm almost quantitative BP conjugation (Supporting Information, Figure S2). First, the carboxylic acid $\text{C}=\text{O}$ stretching band at 1731 cm^{-1} disappears almost completely after BP conjugation with a seemingly proportional increase of the $\text{C}=\text{O}$ amide band at 1653 cm^{-1} . And second, subtracting the spectrum of MeO-PEG(5)-COOH (PEG(5)-COOH) reveals peaks at 1093 cm^{-1} and 962 cm^{-1} , characteristic of $\text{P}=\text{O}$ and $\text{P}-\text{O}$ bond stretching, respectively. In addition, ^{31}P NMR shows a single peak at 13.45 ppm , characteristic of bisphosphonates and unequivocally confirming the success of the conjugation reaction. Furthermore, the presence of phosphorus in PEG(5)-BP, and not in PEG(5)-COOH, was confirmed using Dittmer–Lester stain studies.

Synthesis of PEG(5)-BP-USPIO. The PEGylation reaction is shown in Scheme 1B. First, oleylamine-coated USPIOs ($5.5 \pm 0.6\text{ nm}$ diameter by transmission electron microscopy (TEM)) were synthesized following a published method.¹⁷ The process of functionalization with PEG-BPs from oleylamine-USPIOs can be performed in high yields in 1 h at RT. This is in contrast to other published methods for PEG functionalization in which heating and/or long reaction times were used.^{18–21} First, the nanoparticles were dispersed in dichloromethane and mixed with an excess of PEG(5)-BP. A high PEG(5)-BP/USPIO ratio (10 mg of PEG(5)-BP/ mg USPIO) was used in order to maximize the packing density of PEG molecules on the surface of the NPs, as it has been shown that high PEG packing density results in particles with higher colloidal stability.¹⁸ The mixture was then sonicated in an open vial using a standard laboratory sonic bath until most of the dichloromethane had evaporated and only a gummy brown residue was left. This residue could then be fully dispersed in water, suggesting the ligand exchange had occurred. To remove oleylamine, the aqueous mixture was washed with hexane several times followed by evaporation of the volatiles using a stream of nitrogen and a rotary evaporator. No USPIOs were detected in the organic washings. The mixture was then filtered using a 220 nm filter to remove any potential aggregates. Visual inspection of the membrane after filtration showed no signs of colored material, suggesting that no aggregates with diameters greater than 220 nm had formed. To remove the nonbound PEG(5)-BP, the mixture was transferred to a centrifugal concentrator with a molecular weight cutoff (MWCO) of 30 kDa , and washed several times with water. This step was used to obtain the pure PEG(5)-BP-USPIOs, but also to concentrate them and to calculate the amount of PEG(5)-BP that had not bound to the surface of the nanoparticles and hence provide us with an indirect estimation of the number of PEG molecules per iron oxide nanoparticle (*vide infra*). The purified PEG(5)-BP-USPIOs in water were transferred and stored in a glass vial.

We should note that PEG(5)-BP is also very effective for coating and stabilizing iron oxide nanomaterials synthesized using standard coprecipitation methods (Supporting Information). The addition of PEG(5)-BP to a dispersion in water of iron oxide nanoparticles, prepared following a well established coprecipitation method,²² resulted in efficient PEGylation after several size-exclusion filtrations to remove unbound polymer. On the other hand, using the same amounts and method, PEG(5)-COOH did not yield stable dispersions. Dynamic light scattering (DLS) studies over 7 days confirmed full stability in saline compared to non-PEGylated ferrofluids. In our hands, however, the oleylamine method of Xu *et al.*¹⁷ yielded, smaller and more monodispersed USPIOs better suited for our purposes.

Characterization of PEG(5)-BP-USPIO. The particles were characterized by TEM, DLS, thermogravimetric analysis (TGA), energy-dispersive X-ray spectroscopy (EDX), X-ray photoelectron spectroscopy (XPS), powder X-ray diffraction (XRD), and IR spectroscopy (Figure 1). In addition, their magnetic properties were investigated using a superconducting quantum interference device–vibrating sample magnetometer (SQUID–VSM) (Supporting Information). TEM provides information about the size of the inorganic core before and after PEGylation. Thus, oleylamine-coated USPIOs had a metallic core with a diameter (D_{TEM}) of $5.5 \pm 0.6\text{ nm}$, based on statistical analysis of 200 particles. After PEGylation, the iron oxide core of PEG(5)-BP-USPIOs remained unchanged with a measured D_{TEM} of $5.5 \pm 0.7\text{ nm}$. The observation that the diameter of the USPIOs does not change after PEGylation demonstrates that BPs do not etch the surface of the iron oxide NPs. This contrasts with the use of other anchor groups such as catechols where etching of the surface of iron oxide nanoparticles has been shown.^{23,24} This is most probably due to the high affinity of some catechols toward Fe^{3+} ions and the remarkably high stability of the complexes formed. In addition, formation of toxic semiquinone radical species has been observed at catechol–iron oxide surfaces.²⁵ In two recent reports, however, Amstad *et al.*, have shown that these adverse effects can be overcome by fine-tuning the electronic properties of these anchors by introduction of a strong electron-withdrawing nitro group to the aromatic ring.^{18,23}

The hydrodynamic diameter (D_{H} , Figure 1C) was measured using DLS in water and saline. In both cases, PEG(5)-BP-USPIO shows a D_{H} of $24 \pm 3\text{ nm}$, and this value remained unchanged for at least 7 months (Supporting Information). An extended 5 kDa PEG polymer chain should have a length of approximately 38 nm . As a consequence, if PEG(5)-BP was fully extended on the surface of the USPIOs, they should have a minimum mean D_{H} of around 80 nm . Thus, given the smaller size found, the PEG polymers must be

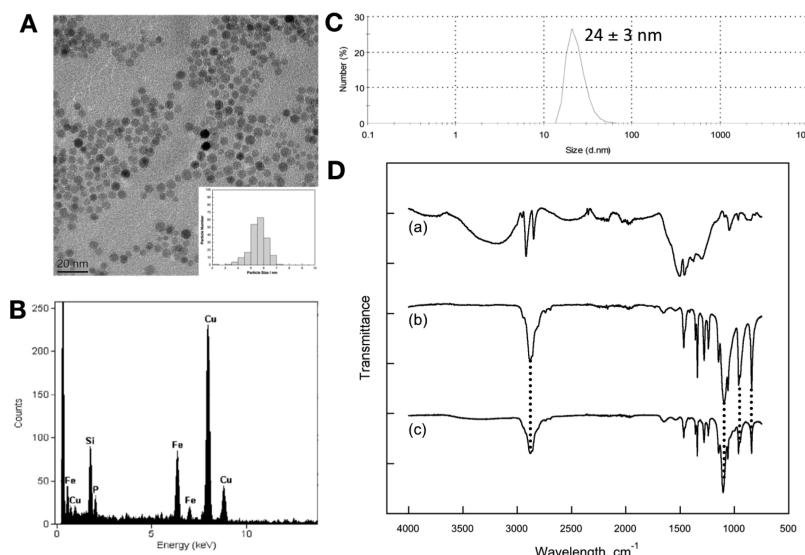


Figure 1. Characterization of PEG(5)-BP-USPIO: (A) TEM micrograph of a dispersion in water. Scale bar is 20 nm wide. Inset is a histogram of the diameter of 200 particles ($D_{\text{TEM}} = 5.5 \pm 0.7 \text{ nm}$); (B) EDX spectrum showing the presence of iron and phosphorus in the sample; (C) DLS showing a hydrodynamic diameter of $24 \pm 3 \text{ nm}$; (D) IR spectra of (a) oleylamine-USPIOS, (b) PEG(5)-BP, (c) PEG(5)-BP-USPIO. Drop lines indicate the vibrations associated with PEG mentioned in the text.

in an expanded coil conformation in which the polymers have folded to $\frac{1}{4}$ of their extended length.²⁶ The density of PEG(5)-BP on the surface of the USPIOS can be estimated using the amount of nonbound PEG(5)-BP recovered after the synthesis of PEG(5)-BP-USPIO (Supporting Information). Thus, our estimations result in density values that range from 76 to 198 PEGs/USPIO. However, given that our calculations of the theoretical maximum number of BP groups that each 5.5 nm USPIO can accommodate is 112 (Supporting Information), the true density is likely to be a value in the range between 76 and 112 PEGs/USPIO, which corresponds to a surface density of 68% to 100%, or 0.80–1.18 PEGs/nm². TGA measurements were carried out to validate these estimations. The results confirm that 67% of the weight of PEG(5)-BP-USPIO is due to PEG(5)-BP, which corresponds to a surface density of 0.9 PEGs/nm² (76%) or 86 PEGs/USPIO (Supporting Information). We note that the high density value found is counterintuitive, particularly when the DLS results suggest the PEG chains are likely to be present as folded extended coils that will impact negatively in the density. However, these calculations assume a flat surface area and recent studies have demonstrated that the curvature of USPIOS and other nanomaterials allows significant higher densities.¹⁸ In addition, sources of error such as the assumption that the particles are homogeneous spheres of 5.5 nm diameter and not taking into account the small variations in diameter/surface areas may also influence our calculations.

IR, EDX, XRD, and XPS spectroscopies were used to identify the presence on PEG(5)-BP after purification and to confirm oleylamine removal. XRD studies (Figure 2) show the characteristic peaks due to iron

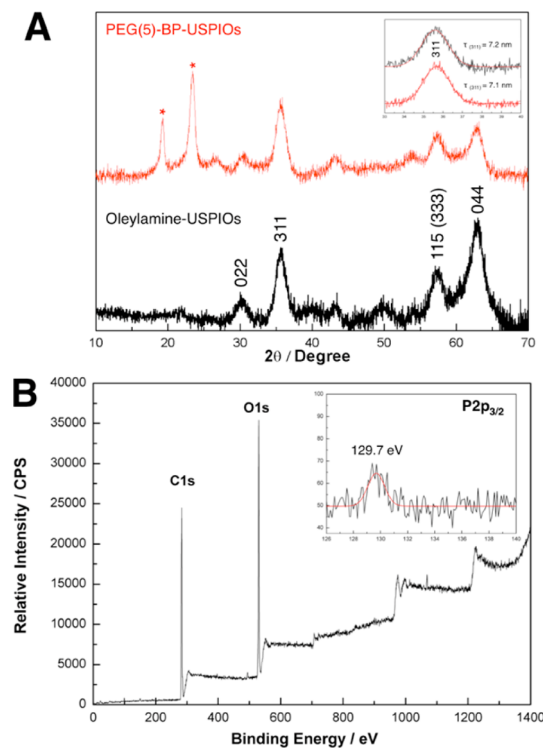


Figure 2. Characterization of PEG(5)-BP-USPIOS. (A) XRD patterns of oleylamine-USPIOS (bottom, black) and PEG(5)-BP-USPIOS (top, red). Peaks corresponding to iron oxide were labeled with their corresponding planes. The inset shows the peak corresponding to the (311) plane and its mean size ($\tau_{(311)}$) calculated using the Scherer equation. The peaks corresponding to PEG(5)-BP ($2\theta = 19.2^\circ$ and 23.3°) have been labeled with an asterisk. (B) XPS spectrum of PEG(5)-BP-USPIOS. The full spectrum shows dominant C1s and O1s signals from the PEG chains on the surface (for a detailed spectrum see Supporting Information). Inset shows the weak but detectable P2p_{3/2} signal arising from the BP group.

oxide as well as PEG (19.2° and 23.3°),^{27,28} which is probably the result of its high density and ordered structure near the surface of the USPIOs. The IR spectra of oleylamine-USPIOs, PEG(5)-BP, and PEG(5)-BP-USPIO are shown in Figure 1D. The presence of characteristic PEG vibrations ($\nu(\text{C}-\text{O}) + \rho(-\text{CH}_2-) = 1096 \text{ cm}^{-1}$; $\rho(-\text{CH}_2-) + \tau(-\text{CH}_2-) = 946 \text{ cm}^{-1}$; $\tau(-\text{CH}_2-) + \nu(\text{C}-\text{O}) = 841 \text{ cm}^{-1}$)²⁹ in the spectrum of PEG(5)-BP-USPIO (Figure 1D-c) confirms the success of the PEGylation. This result, however, does not confirm complete oleylamine removal, despite that the high PEG densities achieved (76%, *vide supra*) strongly suggest that at least most has been displaced. The expected shift of $-\text{PO}_3$ vibrations upon metal binding was not observed due to the above-mentioned overlap with the more intense signals from the PEG methylene groups. EDX studies show the presence of phosphorus in the TEM of PEG(5)-BP-USPIO indicating the presence of the BP group (Figure 1B). This is also supported by XPS, where a signal at a binding energy of 129.7 eV, corresponding to $\text{P}(2\text{p}_{3/2})$ was observed (Figure 2B). Similar signals have been observed with other metallic surface-bound bis- and monophosphonates.^{30,31} The XPS spectrum also shows characteristic C(1s) PEG peaks at 282–286 eV, further confirming its presence.

PEG coatings are known to give rise to nanoparticles with a neutral surface charge. This is an important factor as it is well established that highly negative NP surfaces favor uptake by RES macrophages while positive surfaces result in plasma protein binding, aggregation, and uptake in lungs and liver.^{32,33} ζ -Potential measurements in phosphate buffered saline (PBS) confirmed a near-zero potential of -1.24 mV , and hence neutral surface charge at physiological pH. The neutral surface of PEG(5)-BP-USPIO as well as the high PEG density found are expected to minimize opsonization and RES uptake and prolong blood half-life. The magnetic properties of PEG(5)-BP-USPIOS were investigated using a SQUID-VSM instrument at 300 K (Figure S6, Supporting Information). The profile demonstrates superparamagnetic behavior and allows us to calculate a mass magnetization at saturation (M_s) of 51 emu/g iron oxide. This value is relatively low compared to that of bulk iron oxide (maghemite ($\gamma\text{-Fe}_2\text{O}_3$, bulk $M_s = 74 \text{ emu/g}$) and magnetite (Fe_3O_4 , bulk $M_s = 98$)), and is consistent with that found with other USPIOS of similar size and *in vivo* magnetic properties.¹⁹

Radiolabeling of PEG(5)-BP-USPIOS. The labeling of PEG(5)-BP-USPIO with a gamma-emitting isotope (^{99m}Tc) was used to study its biodistribution *in vivo* using SPECT imaging. We have recently shown that BPs can be used to radiolabel the metal ions on the surface of iron oxide nanoparticles with PET and SPECT isotopes without affecting their coatings or surface properties.^{13,14} This is due to the remarkably low quantities in which BPs can be radiolabeled (micrograms), while still providing a strong signal from the high

energy photons they emit.³⁴ As a consequence, the radiolabeled BPs are present in a much lower quantity than the NPs and coating molecules. Hence, even in the event that the radiolabeled BP displaces molecules of the coating or binds to gaps on the inorganic core, the changes would be so small (quantitatively and qualitatively) that their colloidal or magnetic properties would not be affected. Here, we used ^{99m}Tc -DPA-ale, a bifunctional BP that we have recently shown can be used to radiolabel iron oxide materials with high *in vitro/vivo* stability.³⁴ Thus, by simply adding a solution of ^{99m}Tc -DPA-ale to a dispersion of PEG(5)-BP-USPIO in saline, radiolabeling yields (RLY) of up to 47% can be obtained after a short reaction time of 10 min. Temperature has a large effect in the RLY obtained, and varies from 2% at 20°C to 25% at 37°C and 47% using a temperature gradient (25 – 90°C over 10 min). Reaction pH (6–9) did not affect RLY. In a previous report, we have shown that ^{99m}Tc -DPA-ale binds rapidly and almost quantitatively to non-coated iron oxide materials at room temperature.¹³ However, in PEG(5)-BP-USPIO, our calculations estimate that approximately 24% of the metallic surface is available for binding (*vide supra*). In addition, it is expected that the PEG layer will limit the accessibility of molecules to the USPIOS. The increased RLY at increasing temperatures is therefore presumed to be an effect of an increased exposure of the less-accessible metallic surface. This can be the consequence of two mechanisms: (1) ligand exchange on the surface or (2) diffusion of ^{99m}Tc -DPA-ale through the PEG layer to reach exposed gaps of the metallic core (Figure 3A). Given the results from the PEG surface density calculations and the high stability of the BP-iron oxide bond,^{13,14,35}–⁴² we believe that the latter mechanism is the most probable, although the former cannot be ruled out.

Purification was achieved using size exclusion chromatography with disposable columns containing Sephadex G-25 medium and size exclusion filters with a 10 kDa MWCO using saline as eluent. Figure 3B shows a typical elution chromatogram from a size exclusion column after radiolabeling PEG(5)-BP-USPIOS at 37°C . As expected from their large size, radiolabeled PEG(5)-BP-USPIOS elute as a sharp peak at 1.5 mL, whereas ^{99m}Tc -DPA-ale elutes as a broader peak at 4 mL. The entire radioactivity was recovered from the column after using 12 mL of eluent, proving the absence of nonspecific binding to the column matrix. The coelution of the first radioactive peak with PEG(5)-BP-USPIOS, clearly identified visually, demonstrates the association between particles and radioactivity (Figure 3B). A centrifugal concentrator was then used to concentrate the sample to the desired volume and to separate the small portion of free ^{99m}Tc -DPA-ale that coeluted with the radiolabeled PEG(5)-BP-USPIOS in the size-exclusion separation. The particles can also be purified with this device without the use of size

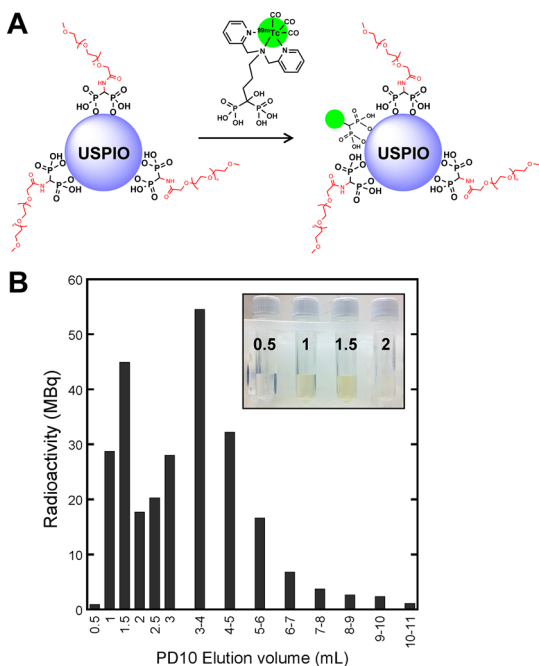


Figure 3. Radiolabeling of PEG(5)-BP-USPIOs with 99m Tc-DPA-ale: (A) radiolabeling scheme (B) size exclusion (PD10) chromatogram of the reaction (please note that 0.5 mL fractions were collected from 0 to 3 mL elution volume, and 1 mL fractions were collected from 3 to 11 mL elution volume). Radiolabeled PEG(5)-BP-USPIOs elute at a peak at 1.5 mL, whereas free 99m Tc-DPA-ale elutes at a broad peak at 4 mL. (The inset is a picture of the first 4 fractions showing the presence of the USPIOs). Fractions containing radiolabeled PEG(5)-BP-USPIOs (0.5–2 mL) were further purified and concentrated using size-exclusion filtration.

exclusion chromatography. It was found, however, that 9% of the radioactivity remained nonspecifically bound to the filters. The cause of this nonspecific binding to the filter remains unknown. DLS studies of radiolabeled PEG(5)-BP-USPIOs after purification and radioactivity decay show no changes in the hydrodynamic size. In addition, 1 H NMR of the residue after evaporation of the size exclusion and filtration fractions/filtrates did not show any detectable PEG peaks. These two results demonstrate that the radiolabeling step does not affect the coating and confirms the low, if any, PEG displacement after radiolabeling.

In Vitro Stability Studies. Several observations confirm the high colloidal stability of the BP-coated USPIOs. First, DLS studies demonstrate that the D_H of PEG(5)-BP-USPIO stored in water or saline for 7 months remains unchanged, with no aggregates forming during this time. In addition, heating dispersions of PEG(5)-BP-USPIOs in saline to 90 °C for 10 min and at 50 °C for 4 h results in no change in D_H or aggregation. Another indication of their stability is given by the number of times PEG(5)-BP-USPIOs can be washed with large volumes of saline and water using 30 kDa molecular weight cutoff filters without changes in D_H (>8 times). This is in contrast to PEG(5)-COOH-USPIOs, synthesized using the same method as PEG(5)-BP-USPIOs, where

complete aggregation occurred after the fourth washing (Supporting Information). Thus, when desorption occurs, PEG molecules (5 kDa) will be removed from the retentate containing the dispersion into the filtrate, eventually inducing the aggregation of the SPIOS. Amstad *et al.* have previously used this method to evaluate the binding reversibility of several PEG coatings on SPIOS, showing that with PEG-COOH and weakly bound PEG-catechols, aggregation occurred between the first and fourth filtration.¹⁸ Irreversible binding, however, was indicated by no changes in D_H after four filtrations with strongly bound catechol–PEG conjugates. Furthermore, the D_H of PEG(5)-BP-USPIOs remained constant after repeating the process at several time points during several months. The lack of binding and stabilization properties of PEG-COOH to oleylamine USPIOs also represents convincing data to rule out the possibility that the PEG polymer may be binding nonspecifically to the alkyl chains, a method that has been successfully used with other systems.⁴³ Stability studies were also carried out with radiolabeled PEG(5)-BP-USPIOs allowing us to measure the stability of the BP-iron oxide bond in human serum. Thus, incubation at 37 °C in human serum shows that after 48 h at physiological temperature and protein and salt concentrations, 94% of the radioactivity remains bound to the USPIOs. This result is consistent with our previous report using dextran-coated SPIOS and other reports that have shown the high stability of the BP-iron oxide bond (more than 4 weeks at pH 7) compared to other anchors such as carboxylates.^{13,40} In addition, PEG(5)-BP-USPIOs were incubated at the same temperature in 10% human serum and DLS measurements at 0, 1, 24, and 48 h were performed, showing no change in D_H . This result not only supports their stability but also indicates that blood serum proteins do not bind to the nanoparticles. We believe this is a consequence of a compact and stable PEG coating and the neutral ζ -potential achieved. Overall, these results show that both BPs, PEG(5)-BP, and 99m Tc-DPA-ale, bind irreversibly to the iron oxide surface of USPIOs leading to ultrastable nanoparticles and supports previous findings from our group and others on the high stability of the BP-iron oxide bond.^{13,14,35–42}

Relaxivity Measurements and *In Vitro* MRI Studies. MRI relaxivity measurements of PEG(5)-BP-USPIOs were performed to evaluate its potential as a MR contrast agent at a clinically relevant high magnetic field (3 Tesla, 3 T). As a comparison, the same measurements were carried out with Feraspin XS, a commercially available carboxydextrans-coated USPIO for preclinical studies with a similar D_H (18 nm).⁴⁴ The longitudinal and transverse relaxation rates ($R_{1,2}, s^{-1}$) were calculated for both samples at different iron concentrations. The data points obtained were fitted to a straight line and the slopes (relaxivity $r_{1,2}, \text{mM}^{-1} \text{s}^{-1}$) calculated.

TABLE 1. USPIOS and Corresponding Nanoparticle Size by TEM, DLS, Nature of the Coating and Relaxation Properties at 3 T. The Entries Have Been Ordered by Increasing r_2/r_1 Ratio

USPIO	D_{TEM} (nm)	D_{H} (nm)	coating	r_1 ($\text{mM}^{-1} \text{s}^{-1}$)	r_2 ($\text{mM}^{-1} \text{s}^{-1}$)	r_2/r_1	medium	T (°C)	ref
PEG(5)-BP-USPIOs	5.5	23	PEG-BP	9.5	28.2	2.97	H_2O	RT	this work
ESION	2.2	-	PEG-PO	4.8	17.5	3.65	H_2O	-	ref 19
VSOP-C184	8.6	19	citrate	8.0	34.0	4.25	H_2O	37	ref 8
ESION	3	15	PEG-PO	4.8	29.2	6.08	H_2O	-	ref 19
Feraspin XS	-	18	carboxydextran	5.4	36.3	6.72	H_2O	RT	this work
Ferucarbotran (Supravist)	3–5	21	carboxydextran	7.3	57.0	7.81	H_2O	37	ref 51, 52
Ferumoxytol (C7228)	6.7	35	carboxymethyldextran	7.5	92.0	12.27	H_2O	37	ref 8
Ferrumoxtran-10 (Sinerem)	4.5	34	dextran + citrate	5.0	66.0	13.20	H_2O	37	ref 46, 48
ESION	12	-	PEG-PO	2.4	58.8	24.50	H_2O	-	ref 19

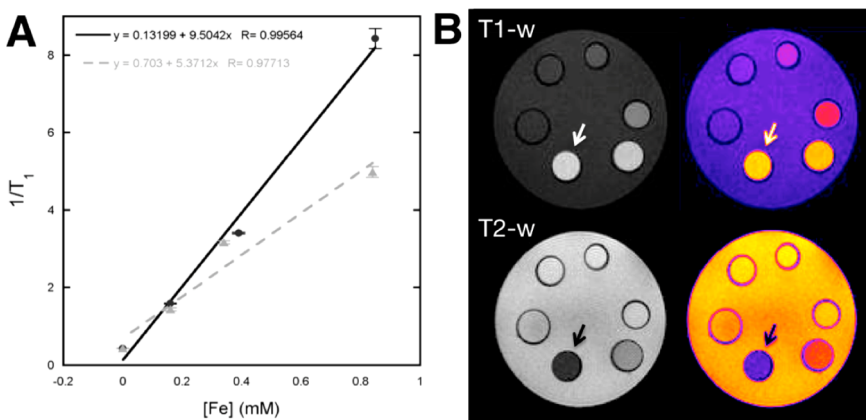


Figure 4. *In vitro* MRI studies of PEG(5)-BP-USPIO: (A) Plot of the relaxation rates ($R_1 = 1/T_1$) as a function of Fe concentration showing the r_1 relaxivities of PEG(5)-BP-USPIO (black circles, $9.5 \text{ mM}^{-1} \text{s}^{-1}$) and Feraspin XS (gray triangles, $5.4 \text{ mM}^{-1} \text{s}^{-1}$); (B) Phantom MRI images (grayscale, left; color scale, right) of PEG(5)-BP-USPIO showing the concentration-dependent effect in T1- (top) and T2- (bottom) weighted sequences. The arrow indicates the most concentrated vial (5.3 mM Fe) and the concentration decreases anticlockwise, with the last vial containing water only.

The values obtained as well as those reported in the literature for other USPIOS at 3T are listed in Table 1. USPIOS can be used to obtain contrast in both T1- and T2-weighted MR imaging. For effective T1 contrast with superparamagnetic iron oxide materials, high r_1 relaxivities and low r_2/r_1 ratios are desirable. On the other hand, high r_2 relaxivities and r_2/r_1 ratios are preferred for T2 contrast. A perusal of Table 1 shows that PEG(5)-BP-USPIOS have optimal properties for efficient T1 contrast, with a high r_1 and low r_2/r_1 ratio of $9.5 \text{ mM}^{-1} \text{s}^{-1}$ and 2.97, respectively. Notably, the relaxivity properties for T1-weighted imaging are 2-fold better than those of commercially available Feraspin XS (measured under the exact same conditions), and compare very favorably with other USPIOS approved for clinical use measured at the same magnetic field and under similar conditions (Table 1, Figure 4). MR imaging of the same samples used for the relaxivity measurements confirms the strong T1 effect and low T2 effect of PEG(5)-BP-USPIOS (Figure 4).

We were impressed by the high r_1 /low r_2 relaxivities obtained at 3 T. It is well established that the r_1 of USPIOS is particularly sensitive to the strengths of the magnets of current MRI scanners. Thus, r_1 tends

to decrease dramatically from 1.5 T scanners to 3 T scanners. On the contrary, r_2 relaxivities remain mostly constant. This behavior can be explained theoretically using the standard relaxation theories for small particles but have also been observed experimentally in many studies with USPIOS.⁴⁵ For example, a decrease of approximately 50% in r_1 ($\text{mM}^{-1} \text{s}^{-1}$) has been observed with Sinerem (1.5 T vs 3 T) (15.5 vs 6.6), VSOP-C184 (14.0 vs 8.0) and Ferumoxytol (15.0 vs 7.5).^{8,46–48} On the other hand r_2 values tend to remain constant (65.0 vs 66.0; 33.4 vs 34.0; 89 vs 92, respectively). Thus, as 3 T MRI scanners are increasingly becoming available in clinics as a result of their improved image resolutions; there is an interest of developing USPIOS that retain high T1 effects at these field strengths. We believe the strong T1 effect of PEG(5)-BP-USPIOS at 3 T is the result of (1) small diameter NP cores of superparamagnetic iron oxide that are known to yield USPIOS with low M_s values and strong T1 effects;^{19,20,49,50} (2) a coating composed of two hydrophilic components, PEG and BP, that facilitate diffusion of water molecules to reach the iron oxide surface and allow the relaxation of their protons; and (3) a stable and compact PEG coating, provided by the strong

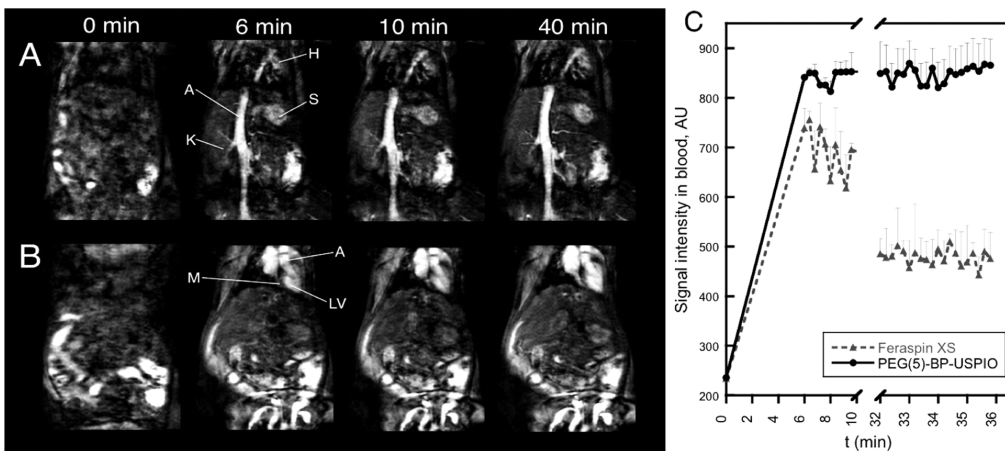


Figure 5. *In vivo* MRI studies with PEG(5)-BP-USPIO: (A, B) T1-weighted images showing the increase in signal from blood in the vessels (A) and the heart (B) at different time points ($t = 0$ min, pre-injection). Labels: H = heart, S = spleen, K = kidney, A = aorta, M = myocardium, LV = left ventricle. (C) Kinetic profile of the MRI signal intensity in blood obtained from PEG(5)-BP-USPIO (black circles, $10 \mu\text{mol Fe/kg}$ dose) and Feraspin XS (gray triangles, $40 \mu\text{mol Fe/kg}$ dose).

BP-iron oxide bond, that prevents aggregation that would increase r_2 and hence the r_2/r_1 ratio.

In Vivo MRI Imaging. The ability of PEG(5)-BP-USPIOS as contrast agent in T1-weighted MRI *in vivo* was assessed using a 3T clinical scanner. The results confirmed the strong T1 effect seen in the *in vitro* studies. Tail vein injection of PEG(5)-BP-USPIOS into a BalbC mouse resulted in a substantial increase in signal from blood that makes vessels, the heart compartments, and other highly vascularized organs such as the spleen visible (Figure 5A,B). Interestingly, the signal intensity in blood remained constant throughout the length of the experiment (40 min), whereas a significant decay of approximately 50% was seen at the end of the experiment when Feraspin XS was used (Figure 5C). Extended blood half-life is an important factor for blood pool MRI agents as it allows the acquisition of high-resolution images and could facilitate diagnosis of a series of conditions such as tumor angiogenesis, aneurysms, and internal bleeding.^{53,54} In addition, low RES uptake and extended circulation times are required when using targeted USPIOS that bind specific receptors.

Another important factor is the dose of contrast agent required to obtain signal enhancement. Remarkably, PEG(5)-BP-USPIOS require a very low dose compared to other USPIOS. The standard dose of USPIOS for MR angiography in human and preclinical studies is $40\text{--}70 \mu\text{mol Fe/kg}$.^{19,55\text{--}57} However, a recent clinical study reported adverse clinical events after administration of USPIOS at $60 \mu\text{mol Fe/kg}$.⁵⁷ The high r_1 relaxivity and low r_2/r_1 ratio of PEG(5)-BP-USPIOS, however, allow us to obtain high signal enhancement with significantly lower doses. In our study, the dose of PEG(5)-BP-USPIOS required to obtain a similar signal enhancement to Feraspin XS was 4 times lower ($10 \mu\text{mol Fe/kg}$ vs $40 \mu\text{mol Fe/kg}$) (Figure 5C). We believe this is a result of the combination of optimal relaxation properties and long blood circulation time. T1-mapping studies of the aorta support this hypothesis. Thus, the

normal relaxation rate (R_1) of blood is $0.74 \pm 0.05 \text{ s}^{-1}$. Forty minutes after injection of PEG(5)-BP-USPIOS, the rate had increased more than 6-fold to $4.78 \pm 1.90 \text{ s}^{-1}$, whereas for Feraspin XS this value was $2.39 \pm 0.33 \text{ s}^{-1}$.

Although most PEG(5)-BP-USPIO remained in the bloodstream for the length of the MRI study, we examined its excretion route using a T2*-weighted gradient echo sequence. This sequence was chosen because it is very sensitive to the accumulation and changes in relaxivity of SPIOS in tissues.⁵⁸ Thus, T2*-weighted imaging and a mapping sequence were acquired before and 50 min after injection of PEG(5)-BP-USPIOS. The images reveal signs of liver accumulation and hence hepatic excretion as expected for a NP of this D_H (Figure S7, Supporting Information). Accumulation starts within the first hour after injection, although the high signal from the blood throughout the experiment suggests that liver uptake must be minimal. Interestingly, SPECT imaging studies with the radiolabeled version of PEG(5)-BP-USPIOS corroborate these results and reveal that liver uptake seems to be related to the slow loss of the coating *in vivo* (*vide infra*).

In Vivo SPECT Imaging. Radiolabeled PEG(5)-BP-USPIO was used to study its biodistribution *in vivo* with the high sensitivity of SPECT imaging and to study the fate of the BP coating. After intravenous injection into Balb/C mice, the animals were imaged at three time points over 3.3 h using a preclinical SPECT/CT scanner (Figure 6A,B). The images and pharmacokinetic profile confirm the behavior seen in the MR imaging study and demonstrate that the majority of PEG(5)-BP-USPIOS circulate in the bloodstream for at least the length of the study as evidenced by the high signal in the heart as well as major blood vessels and vascular organs. A pharmacokinetic profile (Figure 6C) shows that the signal of vascular organs reaches maximum concentration before the first 45 min followed by an elimination phase after 80 min. On the other hand

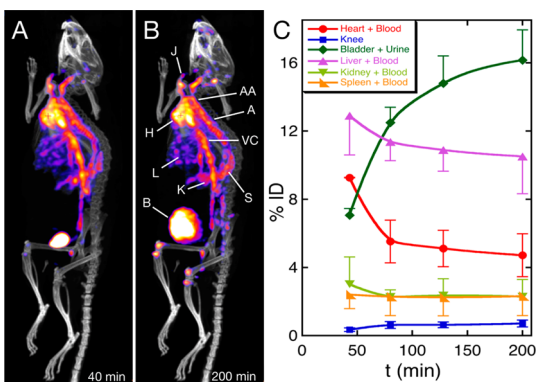


Figure 6. *In vivo* SPECT-CT studies with PEG(5)-BP-USPIO: (A, B) Maximum intensity projection SPECT-CT images after *iv* injection of radiolabeled (^{99m}Tc) PEG(5)-BP-USPIO at the first (A, 40 min) and last (B, 200 min) time points. (Labels: H = heart, J = jugular vein, AA = aortic arch, A = aorta, VC = vena cava, L = liver, K = kidney, S = spleen, B = bladder). (C) Pharmacokinetic profile as obtained by quantification of the signal from several tissues showing the changes in the percentage of the injected dose (% ID) as a function of time. Data represent the mean \pm SD ($n = 2$ mice).

there is a continuous signal increase in nonvascular organs such as the bladder and bones (knee), which is due to free ^{99m}Tc -DPA-ale, as a result of the decomposition of PEG(5)-BP-USPIOS (*vide infra*). Interestingly the images at the first time point reveal a high signal from the bladder that may be the result of small population of USPIOS that were small enough to be excreted with the urine.³² Another possibility is that a large fraction of ^{99m}Tc -DPA-ale (~7%ID) detaches soon after injection. There are some indications, however, that this option is less likely. For example, if 7%ID suddenly detached from the iron oxide nanoparticles once in the bloodstream, we would expect to see a much higher bone uptake in the first time point, as we find when we inject ^{99m}Tc -DPA-ale alone.³⁴ Also, a sudden breaking of the BP-iron oxide bond after injection is not in agreement with the slow rate of BP release found throughout the rest of the study and the *in vitro* stability studies. Another possibility is that there is a large proportion of nonspecifically bound radiolabeled BP in the injected solution but this is unlikely after the extensive purification and characterization experiments. In addition, urine analyses with PEG(5)-BP-USPIOS at the end of the imaging study support the presence of radiolabeled nanoparticles (Supporting Information).

The slope of the elimination phase in the heart allows us to calculate a blood half-life ($t_{1/2}$) of 178 min (2.97 h), assuming first-order single compartment pharmacokinetics. Interestingly there is no sign of accumulation in the liver. On the other hand, injection of radiolabeled Feraspin XS reveals that the activity accumulates solely in the liver and bladder 50 min after injection (Figure S8, Supporting Information).⁵⁹ This is expected for Feraspin XS and other dextran-coated USPIOS, as this polysaccharide is avidly taken by macrophages, providing a useful method to target

these NPs to macrophage-rich tissues.^{60,61} This result is also consistent with the MRI experiments using Feraspin XS in which there was a 50% reduction of signal from the blood in the first 30 min (*vide supra*). Other clinically approved dextran-coated USPIOS also display short blood half-lives in mice (e.g., Sinerem, 18 min).⁸

The SPECT images did not show significant liver uptake. On the other hand, the T2*-weighted MRI studies reveal signs of liver accumulation (Supporting Information, Figure S7). We believe this is the result of a slow loss of the BP-based coating. We base this proposal on the fact that during the 3.3 h-long SPECT study the images show a slow increase in bone uptake which is the result of the release of ^{99m}Tc -DPA-ale into the bloodstream (Figure 6B).³⁴ Thus, as both PEG(5)-BP and ^{99m}Tc -DPA-ale share a BP anchoring group, it is reasonable to assume that PEG(5)-BP is also being released. This would result in USPIO aggregation and facilitate RES uptake of the “naked” NPs which are only detectable by T2*-weighted MRI, and not SPECT scanning. Interestingly, the *in vitro* stability studies in human serum revealed almost no degradation after 48 h at 37 °C (*vide supra*). This implies that the slow release of the BP components *in vivo* may be a consequence of the action of soft tissues. The SPECT images also reveal that there is a significant uptake in the kidneys. Thus, it is possible that the BPs detach from the USPIOS by the action of the kidneys. This is supported by the fact that kidney uptake is clearly seen in the SPECT images (Figure S9, Supporting Information and Figure 6), whereas no kidney retention is observed after injection of ^{99m}Tc -DPA-ale alone.³⁴ In addition, the amount of radioactivity in the urine increased during the imaging experiment. Further experiments are needed to clarify the role of the kidneys and other tissues in the excretion and metabolism of PEG(5)-BP-USPIO. However, a preliminary analysis of the urine by size-exclusion chromatography at the end of the study (3.3 h) was performed. Figure S10 (Supporting Information) shows that most of the activity elutes as a broad peak in the small-molecule area. TLC and hydroxyapatite-binding studies confirmed this band corresponds to ^{99m}Tc -DPA-ale. Thus, if renal metabolism is occurring it seems that, once the BPs are released, a fraction of the radioactivity is excreted in the urine while another is recycled back into the bloodstream, where it binds to bone. Renal excretion and recirculation of BPs has been observed for other BPs.⁶² Interestingly, there is also a small but detectable peak that elutes at the same elution volume as radiolabeled PEG(5)-BP-USPIOS, suggesting a small fraction of particles of very small size are excreted intact.

CONCLUSIONS

We have described the synthesis of a PEG polymer containing a bisphosphonate anchor (PEG(5)-BP) for strong binding to the surface of iron oxide materials

such as USPIO NPs. PEG(5)-BP is capable of generating hydrophilic SPIOs using a simple and fast method. Using this method, we have synthesized a colloidally stable PEGylated USPIO (PEG(5)-BP-USPIO) that can be stored as a dispersion in water or saline for at least 7 months without changes in D_H . PEG(5)-BP-USPIOS can be used as an effective contrast agent for T1-weighted imaging, which is the preferred method of obtaining contrast in MRI. We attribute this effect to its high r_1 and low r_2 relaxivities, a result of the optimal size of the superparamagnetic iron oxide core and stable hydrophilic coating (PEG(5)-BP) that prevents aggregation. To the best of our knowledge, these are the highest r_1 and lowest r_2/r_1 (2.97) reported to date at these conditions ($B_0 = 3$ T). *In vivo* studies demonstrate the high potential of PEG(5)-BP-USPIOS as a contrast agent for MRI angiography. After intravenous injection in mice the blood relaxation rate and hence its signal increased 6-fold for the duration of the experiment, allowing the visualization of blood vessels and vascular organs with high spatial definition. In addition, its improved relaxivities allow the use of a lower dose (4-fold) of contrast agent compared to other USPIOS to obtain a similar signal enhancement. The MRI study revealed minor accumulation of USPIOS in the liver. PEG(5)-BP-USPIOS can also be labeled using a radiolabeled BP, ^{99m}Tc -DPA-ale, that allows tracking of the NPs using SPECT imaging with high sensitivity and quantification capabilities. The *in vivo* imaging study confirmed the MRI results, showing long blood circulation times

($t_{1/2} = 2.97$ h). The SPECT study also provided important information about the fate of PEG(5)-BP-USPIOS and its components. ^{99m}Tc -DPA-ale is being released into the urine and the bloodstream (but only slowly) and leads us to hypothesize that the same may be occurring to PEG(5)-BP. Interestingly, uptake in the kidneys suggest this organ is playing a role in the decomposition of PEG(5)-BP-USPIOS. Further studies, however, are warranted to understand its excretion properties.

This work demonstrates that the surface functionalization with PEG-BPs is an effective method for developing highly stable USPIOS with low RES uptake and long blood circulation times, which are the major limitations in the development of targeted USPIOS for biomedical imaging. This method could be extended to other inorganic nanomaterials of interest in biomedical imaging and engineering to which we have recently shown BPs bind very strongly.¹⁴ Furthermore, we believe PEG(5)-BP-USPIOS represent a promising platform for the development of agents for multimodal medical imaging. These compounds could find applications with the new generation of multimodal clinical scanners (*i.e.*, PET-MR) in which the nuclear imaging capabilities of these agents could be synergistically combined with MRI to improve the information obtained. We expect that targeted probes based on PEG(5)-BP-USPIOS could provide better detectability and quantification capabilities of vascular targets involved in cardiovascular and oncologic diseases.

EXPERIMENTAL SECTION

Materials and Methods. Reagents were obtained from commercial sources and used as received unless otherwise noted. MeO-PEG-COOH ($M_p = 5118$ Da, $D = 1.02$) was purchased from Iris Biotech GmbH (Germany). Organic solvents were of HPLC grade. Dipicolylamine-alendronate (DPA-ale) and ^{99m}Tc -DPA-ale were synthesized as previously reported.³⁴ NMR spectra were obtained using a Bruker Avance 400 at 20 °C in CDCl_3 (Cambridge Isotope Laboratories). ^1H resonances were referenced to the residual protic impurity of the solvent (δ_H 7.26 ppm). ^{31}P resonances were referenced to an external solution of 85% H_3PO_4 (δ_P 0 ppm). Water (type I, 18.2 MΩ·cm) was obtained from an ELGA Purelab Option-Q system. Human serum from human male AB plasma was obtained from Sigma-Aldrich. Na[$^{99m}\text{TcO}_4$] in physiological saline was obtained from a $^{99}\text{Mo}/^{99m}\text{Tc}$ generator at the Radiopharmacy at Guy's and St Thomas' Hospital NHS Trust, London, UK. For TLC studies, silica gel 60 F₂₅₄ glass plates (2.5 cm × 7 cm, Merck KGaA, Germany) were used. TLC plates were scanned with a Mini-Scan TLC scanner equipped with a FC3600 detector of γ photons (Lablogic, UK). Radioactivity in samples was measured with a CRC-25R dose calibrator (Capintec, USA) or a 1282 CompuGamma gamma counter (LKB Wallac, Finland). [$^{99m}\text{Tc}(\text{CO})_3(\text{H}_2\text{O})_3$]⁺ was synthesized using Isolink kits (Mallinckrodt Medical B.V., St. Louis, MO, USA). Size-exclusion filters (Vivaspin) and columns (PD10) were obtained from GE Healthcare, UK. IR studies were performed with a Spectrum 100 spectrometer (Perkin-Elmer, USA) equipped with a universal ATR sampling accessory. The concentrations of iron in the dispersions of SPIO nanoparticles were calculated by ICP-MS (Mass Spectrometry Service, King's College London) after digestion in nitric acid (TraceSelect Ultra,

Sigma Aldrich) for 16 h. Millex IC 0.22 μm hydrophilic 13 mm PTFE filters (Millipore, USA) were used throughout this study. Samples for transmission electron microscopy (TEM) were prepared by evaporation of a drop of the aqueous colloidal suspensions onto a carbon-coated copper grid (200 mesh, Agar Scientific, UK). TEM and energy-dispersive X-ray spectrometry (EDX) were obtained from a Tecnai T20 instrument (FEI, USA) with a LaB6 filament operating at 200 kV and equipped with a Genesis system EDAX spectrometer (EDAX, USA), or a Tecnai F20 200 kV FEGTEM fitted with an Orius SC600 CCD camera (Gatan, USA) and an 80 mm² X-Max SDD EDX detector (Oxford Instruments, UK). X-ray photoelectron spectra (XPS) were recorded using a Kratos AXIS ULTRA with monochromated Al K α radiation (10 kV anode potential, 15 A emission current) in fixed analyzer transmission mode (80 eV pass energy). Dynamic light scattering (DLS) and zeta-potential were performed with a Zetasizer Nano ZS instrument (Malvern Instruments, UK) at 25 °C. Thermogravimetric analysis (TGA) was performed under N_2 flow (60 mL/min) with a heating rate of 10 °C/min using a TA SDT-600 thermogravimetric analyzer. X-ray powder diffraction (XRD) was recorded on a Bruker D8 Advance powder diffractometer with a Cu K α X-ray source ($\lambda = 1.54058$ Å) operating at 40 kV and 40 mA and a Sol-X detector. Magnetization data was obtained with a MPMS SQUID-VSM instrument by Quantum Design (San Diego, USA) at 300 K.

Synthesis of Oleylamine-Coated USPIO. Oleylamine-coated USPIOS were synthesized using a slight variation of the method of Hou, Gao and Sun.¹⁷ Fe(acac)₃ (1.042 g) was added to a mixture 15 mL of benzyl ether and 15 mL of oleylamine. The solution was then dehydrated at 170 °C for 1 h under a N_2 flow followed by a temperature increase to 260 °C over a period of

15 min, after which the heating appliance was removed. The solution was left to cool to room temperature and the iron oxide NPs precipitated upon the addition of 24 mL of ethanol, followed by centrifugation at 7000 rpm for 4 min. The supernatant was discarded and the process repeated with another 20 mL of ethanol, then a further 48 mL. The purified nanoparticles were left to dry overnight and characterized by TEM ($D_{TEM} = 5.5 \pm 0.6$ nm, based on statistical analysis of 200 particles) and DLS ($D_H = 7 \pm 3$ nm, measured in dichloromethane).

Synthesis of PEG(5)-BP. MeO-PEG-COOH (400 mg, 7.8×10^{-5} mol) ($M_p = 5118$ Da, $D = 1.02$) was dissolved in anhydrous dichloromethane (DCM) (2 mL) and cooled to 0 °C under N₂. Dicyclohexylcarbodiimide (DCC) (1.5 eq, 24 mg) was then added, and the mixture was stirred at this temperature for 5 min before tetraethyl aminomethyl-bisphosphonate^{15,16} (1 eq, 24 mg) was added. The reaction solution was left stirring under N₂ at room temperature for 16 h resulting in the appearance of a large amount of a white precipitate. The solution was filtered through Celite, evaporated to $\frac{2}{3}$ of the initial volume and left at 4 °C for 4 h to induce precipitation of any residual precipitate. After another filtration through Celite, the mixture was evaporated to dryness, dissolved in 2 mL of anhydrous DCM and cooled to 0 °C under N₂. Trimethylsilyl bromide (TMBS) (15 eq, 145 μL) was added dropwise and the reaction solution was left stirring at room temperature for 48 h. At this stage, DCM and TMBS were evaporated and the residue was dissolved in 3 mL of MeOH and left stirring for 1.5 h. The solvent was evaporated and the residue dissolved in 5 mL of H₂O, followed by dialysis overnight using a membrane with a molecular weight cutoff of 3500 Da. The product was then lyophilized to give ~400 mg of product as a white powder. ¹H NMR (400 MHz, CDCl₃, 298 K) δ_H (ppm): 3.64 (s, -(CH₂-CH₂-O)-); ³¹P{¹H} NMR (161.9 MHz, CDCl₃, 298 K) δ_P (ppm): 13.45. IR ν(cm⁻¹) 2882, 1653, 1541, 1466, 1359, 1341, 1279, 1241, 1146, 1096, 1060, 960, 946, 841. The presence of P was further confirmed by spotting a TLC plate with a sample of the product and staining using Dittmer–Lester dye, resulting in the appearance of a blue color.

Synthesis of PEG(5)-BP-USPIO. Oleylamine-coated USPIOS (2 mg) and PEG(5)-BP (20 mg) were added to 2 mL of DCM in an open glass vial, and the mixture was sonicated until the solvent evaporated (~15 min). To the remaining residue was added 4 mL of water resulting in a clear brown solution. This mixture was washed with 4 mL of hexanes to remove oleylamine. This process was repeated two more times followed by removal of hexanes by evaporation. The final mixture was filtered through a 0.2 μm hydrophilic PTFE filter, followed by several cycles of washing/concentrating using a Vivaspin 2 centrifugal filter (30 kDa molecular weight cutoff) using water to remove excess PEG(5)-BP. The final amber solution was removed from the filter and stored at 4 °C in a glass vial. TEM ($D_{TEM} = 5.5 \pm 0.7$ nm, based on statistical analysis of 200 particles); DLS ($D_H = 24 \pm 3$ nm, measured in water or saline); IR ν(cm⁻¹) 2882, 1653, 1537, 1466, 1359, 1342, 1279, 1241, 1145, 1105, 1060, 963, 842; EDX (keV) 2.145 (P), 6.404 (Fe), 7.058 (Fe); XRD (2θ, deg) 30.08, 35.43, 37.06, 56.96, 62.35; XPS (eV) 129.7 (P2p_{3/2}), 282.2, 283.5, 286.2 (C1s), 529.7 (O1s), 708 (Fe2p_{3/2}).

Radiolabeling of PEG(5)-BP-USPIOS. To a dispersion of PEG(5)-BP-USPIOS (26 mM Fe) in saline was added 100–1000 MBq of ^{99m}Tc-DPA-ale. The mixture was mixed and incubated at different temperatures and pH values in a sealed vial. For best radiolabeling results (47% radiochemical yield), the reaction was heated from 25 to 90 °C during 10 min at pH 7. The reaction solution was cooled to room temperature, and the contents were separated using a PD-10 column using saline as eluent. Radiolabeled PEG(5)-BP-USPIOS elute at a peak centered at 1.5 mL, whereas nonbound ^{99m}Tc-DPA-ale elutes as a broader band at 4 mL. Radiolabeled PEG(5)-BP-USPIOS can be further purified and concentrated to the desired volume using a centrifugal size-exclusion filter with a molecular weight cutoff of 10 kDa (note that around 9% nonspecific binding to the filters was found).

In Vitro Stability Studies in Human Serum. To assess the *in vitro* stability of radiolabeled PEG(5)-BP-USPIOs in human serum, a 20 μL aliquot containing approximately 100 kBq of ^{99m}Tc in saline was incubated in human serum (500 μL) at 37 °C and

constant shaking for 48 h. At the end of the experiment, the samples were filtered using the size-exclusion filters (MWCO = 10 kDa) and the radioactivity of the filtrate and retentate measured in a gamma-counter. Thus, if ^{99m}Tc-DPA-ale dissociates from the USPIOS, it will elute with the filtrate. It was found that after 48 h of incubation time at 37 °C, 6% of the radioactivity eluted with the filtrate and 94% remained bound to the USPIOS. The radioactivity in the filtrate was identified as ^{99m}Tc-DPA-ale by TLC and hydroxyapatite-binding studies.^{13,34}

In Vivo Studies. *In vivo* studies were carried out in accordance with British Home Office regulations governing animal experimentation. Male Balb/c mice (8–10 weeks old) were used. Before the imaging procedure and contrast agent administration, mice were anesthetized with isoflurane and kept under its influence for the duration of the experiment (maximum 4 h) and culled by cervical dislocation at the end of the imaging session. The contrast agents used were injected intravenously through the tail vein using 0.5 mL insulin syringes. The doses used in these studies were 10 μmol Fe/kg (20 MBq of ^{99m}Tc) in 100 μL (PEG(5)-BP-USPIOS) or 40 μmol Fe/kg (3 MBq of ^{99m}Tc) in 100 μL saline (Feraspin XS).

MR Imaging. *In vivo* MR imaging and relaxivity calculations were performed using a 3T Philips Achieva MR scanner (Philips Healthcare, Best, The Netherlands) equipped with a clinical gradient system (30 mT m⁻¹, 200 mT/m/ms) and a single-loop surface coil (diameter = 47 mm). Anesthesia was induced with 5% and maintained with 1–2% isoflurane during the MRI experiments. Mice were imaged in prone position. Dynamic contrast enhanced (DCE) magnetic resonance angiography (MRA), and T1 and T2* mapping protocols were acquired before and after injection of the nanoparticles. Following a 3D GRE scout scan, coronal 3D fast-field echo DCE-MRA images were acquired with TR = 10 ms, TE = 4.2 ms, flip angle = 40°, FOV = 40 × 36 × 12 mm³, acquired matrix = 160 × 144, slice thickness = 0.5 mm, resolution = 0.25 mm × 0.25 mm, reconstructed resolution = 0.1 mm × 0.1 mm, slice number = 25, averages = 1, temporal resolution = 20 s, number of dynamic scans = 20, duration = 6.7 min.

T1 mapping was performed using a sequence that employs two nonselective inversion pulses with inversion times ranging from 20 to 2000 ms, followed by eight segmented readouts for eight individual images. The two imaging trains result in a set of 16 images per slice with increasing inversion times. For T1 mapping the acquisition parameters were: TR = 5.8 ms, TE = 2.7 ms, flip angle = 10°. FOV = 31 × 31 × 13 mm³, acquired matrix = 80 × 77, measured slice thickness = 0.5 mm, acquired resolution = 0.4 mm × 0.4 mm, reconstructed resolution = 0.12 mm × 0.12 mm, slices = 26, averages = 1.

T2* mapping was performed using a 3D fast-field echo sequence. Coronal images were acquired with TR = 248 ms, TE = 4.6 ms, echo spacing = 6.9 ms, six echoes, flip angle = 25°, FOV = 31 × 31 × 13 mm³, acquired matrix = 77 × 77, acquired resolution = 0.41 mm × 0.41 mm, reconstructed resolution = 0.11 mm × 0.11 mm, slice thickness = 0.5 mm, slices = 26, averages = 1. Similar acquisition protocols were used to scan vials containing different concentrations of the nanoparticles to calculate the r_1 and r_2 relaxivities.

MR Image Analysis. MR images were analyzed using the software Osirix (OsiriX Foundation, Geneva, Switzerland). The DCE-MRA images were used to monitor the changes in the signal intensity of blood before and after injection of the nanoparticles. A region of interest (ROI) was manually drawn in the inferior vena cava and propagated over the different time points. T1 mapping images were used to calculate the relaxation rate (R_1) of the liver and blood on a pixel-by-pixel basis using in house software (Matlab, Natick, MA).⁶³ Similarly, the T2* mapping images were used to calculate the relaxation rate (R_2^*) of the corresponding tissues.

SPECT-CT Imaging. SPECT-CT images were obtained with a NanoSPECT/CT PLUS preclinical animal scanner (Mediso, Hungary) equipped with four heads, each with nine 1 mm pinhole collimators, in helical scanning mode in 20 projections over 20 min. The CT images were obtained with a 45 kV X-ray source, 1000 ms exposure time in 180 projections over 10 min. Images were reconstructed in a 256 × 256 matrix using the

HiSPECT (Scivis GmbH) reconstruction software package, and fused using InVivoScope (IVS) software (Bioscan, France). Quantification was performed by selecting the desired organs as regions of interest (ROI) using the quantification tool of the IVS software.

Conflict of Interest: The authors declare no competing financial interest.

Supporting Information Available: Synthesis of PEGylated USPIOS obtained using a coprecipitation method; attempted synthesis of PEG-COOH-USPIO; IR characterization of PEG-BP; calculations of PEG density, including TGA; XPS spectra; DLS studies; magnetic properties of PEG(5)-BP-USPIOS; T2* mapping of PEG(5)-BP-USPIOS; SPECT-CT images of radiolabeled Feraspin XS; kidney uptake SPECT-CT images of radiolabeled PEG(5)-BP-USPIOS and size-exclusion chromatography urine analysis. This material is available free of charge via the Internet at <http://pubs.acs.org>.

Acknowledgment. This work was funded by The Centre of Excellence in Medical Engineering funded by the Wellcome Trust and EPSRC under Grant No. WT 088641/Z/09/Z and the King's College London and UCL Comprehensive Cancer Imaging Centre funded by the CRUK and EPSRC in association with the MRC and DoH (England). L.S. is supported by a EPSRC DTA Ph.D. studentship. L.K.M. is supported by a Cancer Research UK, and P.A.W. is supported by a Harris Studentship. We thank the Wellcome Trust for an equipment grant for the purchase of the SPECT-CT scanner, NanoPET Pharma for the generous gift of Feraspin XS, Covidien for providing us with Isolink kits, Lea Ann Dailey (Institute of Pharmaceutical Science, KCL) for access to the DLS instrument, Steve Clark for assistance in the *in vivo* studies, the staff at the Radiopharmacy at Guys Hospital in London for the radionuclide, and Alice Warley and the Centre for Ultrastructural Imaging (CUI) at KCL for TEM imaging.

REFERENCES AND NOTES

- Chen, X. *Nanoplatform-Based Molecular Imaging*; Wiley: Hoboken, NJ, 2011; p xviii, 823 p.
- Welch, M. J.; Hawker, C. J.; Wooley, K. L. The Advantages of Nanoparticles for PET. *J. Nucl. Med.* **2009**, *50*, 1743–1746.
- Misri, R.; Saatchi, K.; Hafeli, U. O. Nanoprobes for Hybrid SPECT/MR Molecular Imaging. *Nanomedicine (London)* **2012**, *7*, 719–33.
- Stark, D. D.; Weissleder, R.; Elizondo, G.; Hahn, P. F.; Saini, S.; Todd, L. E.; Wittenberg, J.; Ferrucci, J. T. Superparamagnetic Iron-Oxide—Clinical Application as a Contrast Agent for MR Imaging of the Liver. *Radiology* **1988**, *168*, 297–301.
- Weissleder, R.; Hahn, P. F.; Stark, D. D.; Elizondo, G.; Saini, S.; Todd, L. E.; Wittenberg, J.; Ferrucci, J. T. Superparamagnetic Iron-Oxide—Enhanced Detection of Focal Splenic Tumors with MR Imaging. *Radiology* **1988**, *169*, 399–403.
- Colombo, M.; Carregal-Romero, S.; Casula, M. F.; Gutierrez, L.; Morales, M. P.; Bohm, I. B.; Heverhagen, J. T.; Prosperi, D.; Parak, W. J. Biological Applications of Magnetic Nanoparticles. *Chem. Soc. Rev.* **2012**, *41*, 4306–4334.
- Laurent, S.; Forge, D.; Port, M.; Roch, A.; Robic, C.; Elst, L. V.; Muller, R. N. Magnetic Iron Oxide Nanoparticles: Synthesis, Stabilization, Vectorization, Physicochemical Characterizations, and Biological Applications. *Chem. Rev.* **2008**, *108*, 2064–2110.
- Modo, M. M. J. J.; Bulte, J. W. M. *Molecular and Cellular MR Imaging*; CRC Press: Boca Raton, FL, 2007.
- Lee, N.; Hyeon, T. Designed Synthesis of Uniformly Sized Iron Oxide Nanoparticles for Efficient Magnetic Resonance Imaging Contrast Agents. *Chem. Soc. Rev.* **2012**, *41*, 2575–2589.
- Weissleder, R.; Stark, D. D.; Engelstad, B. L.; Bacon, B. R.; Compton, C. C.; White, D. L.; Jacobs, P.; Lewis, J. Superparamagnetic Iron-Oxide—Pharmacokinetics and Toxicity. *Am. J. Roentgenol.* **1989**, *152*, 167–173.
- Jokerst, J. V.; Lobovkina, T.; Zare, R. N.; Gambhir, S. S. Nanoparticle PEGylation for Imaging and Therapy. *Nano med. Nanotechnol., Biol., Med.* **2011**, *6*, 715–728.
- Amstad, E.; Textor, M.; Reimhult, E. Stabilization and Functionalization of Iron Oxide Nanoparticles for Biomedical Applications. *Nanoscale* **2011**, *3*, 2819–2843.
- de Rosales, R. T. M.; Tavare, R.; Glaria, A.; Varma, G.; Protti, A.; Blower, P. J. 99mTc-Bisphosphonate-Iron Oxide Nanoparticle Conjugates for Dual-Modality Biomedical Imaging. *Bioconjugate Chem.* **2011**, *22*, 455–465.
- de Rosales, R. T. M.; Tavare, R.; Paul, R. L.; Jauregui-Osoro, M.; Protti, A.; Glaria, A.; Varma, G.; Szanda, I.; Blower, P. J. Synthesis of 64Cu(II)-Bis(dithiocarbamatebisphosphonate) and Its Conjugation with Superparamagnetic Iron Oxide Nanoparticles: *In Vivo* Evaluation as Dual-Modality PET-MRI Agent. *Angew. Chem., Int. Ed.* **2011**, *50*, 5509–5513.
- Kantoci, D.; Denike, J. K.; Wechter, W. J. Synthesis of Aminobisphosphonate. *Synth. Commun.* **1996**, *26*, 2037–2043.
- Kubicek, V.; Rudovsky, J.; Kotek, J.; Hermann, P.; Elst, L. V.; Muller, R. N.; Kolar, Z. I.; Wolterbeek, H. T.; Peters, J. A.; Lukes, I. A Bisphosphonate Monoamide Analogue of DOTA: A Potential Agent for Bone Targeting. *J. Am. Chem. Soc.* **2005**, *127*, 16477–16485.
- Xu, Z. C.; Shen, C. M.; Hou, Y. L.; Gao, H. J.; Sun, S. S. Oleylamine as Both Reducing Agent and Stabilizer in a Facile Synthesis of Magnetite Nanoparticles. *Chem. Mater.* **2009**, *21*, 1778–1780.
- Amstad, E.; Gillich, T.; Bilecka, I.; Textor, M.; Reimhult, E. Ultrastable Iron Oxide Nanoparticle Colloidal Suspensions Using Dispersants with Catechol-Derived Anchor Groups. *Nano Lett.* **2009**, *9*, 4042–4048.
- Kim, B. H.; Lee, N.; Kim, H.; An, K.; Park, Y. I.; Choi, Y.; Shin, K.; Lee, Y.; Kwon, S. G.; Na, H. B.; et al. Large-Scale Synthesis of Uniform and Extremely Small-Sized Iron Oxide Nanoparticles for High-Resolution T1 Magnetic Resonance Imaging Contrast Agents. *J. Am. Chem. Soc.* **2011**, *133*, 12624–12631.
- Tromsdorf, U. I.; Bruns, O. T.; Salmen, S. C.; Beisiegel, U.; Weller, H. A Highly Effective, Nontoxic T-1 MR Contrast Agent Based on Ultrasmall PEGylated Iron Oxide Nanoparticles. *Nano Lett.* **2009**, *9*, 4434–4440.
- Hu, F. Q.; Wei, L.; Zhou, Z.; Ran, Y. L.; Li, Z.; Gao, M. Y. Preparation of Biocompatible Magnetite Nanocrystals for *In Vivo* Magnetic Resonance Detection of Cancer. *Adv. Mater.* **2006**, *18*, 2553–+.
- Kang, Y. S.; Risbud, S.; Rabolt, J. F.; Stroeven, P. Synthesis and Characterization of Nanometer-size Fe3O4 and Gamma-Fe2O3 Particles. *Chem. Mater.* **1996**, *8*, 2209–2211.
- Amstad, E.; Gehring, A. U.; Fischer, H.; Nagaiyanallur, V. V.; Hahner, G.; Textor, M.; Reimhult, E. Influence of Electro-negative Substituents on the Binding Affinity of Catechol-Derived Anchors to Fe3O4 Nanoparticles. *J. Phys. Chem. C* **2011**, *115*, 683–691.
- Yuen, A. K. L.; Hutton, G. A.; Masters, A. F.; Maschmeyer, T. The Interplay of Catechol Ligands with Nanoparticulate Iron Oxides. *Dalton Trans.* **2012**, *41*, 2545–2559.
- Shultz, M. D.; Reveles, J. U.; Khanna, S. N.; Carpenter, E. E. Reactive Nature of Dopamine as a Surface Functionalization Agent in Iron Oxide Nanoparticles. *J. Am. Chem. Soc.* **2007**, *129*, 2482–2487.
- Allen, C.; Dos Santos, N.; Gallagher, R.; Chiu, G. N. C.; Shu, Y.; Li, W. M.; Johnstone, S. A.; Janoff, A. S.; Mayer, L. D.; Webb, M. S.; et al. Controlling the Physical Behavior and Biological Performance of Liposome Formulations through Use of Surface Grafted Poly(ethylene glycol). *Biosci. Rep.* **2002**, *22*, 225–250.
- Wang, Q.; Dong, Z. F.; Du, Y. M.; Kennedy, J. F. Controlled Release of Ciprofloxacin Hydrochloride from Chitosan/Polyethylene Glycol Blend Films. *Carbohydr. Polym.* **2007**, *69*, 336–343.
- Yadav, A. K.; Mishra, P.; Mishra, A. K.; Mishra, P.; Jain, S.; Agrawal, G. P. Development and Characterization of Hyaluronic Acid-Anchored PLGA Nanoparticulate Carriers of Doxorubicin. *Nanomed. Nanotechnol., Biol., Med.* **2007**, *3*, 246–57.
- DiNoto, V. A Novel Polymer Electrolyte Based on Oligo(ethylene glycol) 600, K2PdCl4, and K3Fe(CN)6. *J. Mater. Res.* **1997**, *12*, 3393–3403.
- Fishbein, I.; Alferiev, I. S.; Nyanguile, O.; Gaster, R.; Vohs, J. M.; Wong, G. S.; Felderman, H.; Chen, I. W.; Choi, H.;

- Wilensky, R. L.; et al. Bisphosphonate-Mediated Gene Vector Delivery from the Metal Surfaces of Stents. *Proc. Natl. Acad. Sci. U.S.A.* **2006**, *103*, 159–64.
31. Das, M.; Mishra, D.; Dhak, P.; Gupta, S.; Maiti, T. K.; Basak, A.; Pramanik, P. Biofunctionalized, Phosphonate-Grafted, Ultrasmall Iron Oxide Nanoparticles for Combined Targeted Cancer Therapy and Multimodal Imaging. *Small* **2009**, *5*, 2883–2893.
 32. Choi, H. S.; Liu, W.; Misra, P.; Tanaka, E.; Zimmer, J. P.; Ipe, B. I.; Bawendi, M. G.; Frangioni, J. V. Renal Clearance of Quantum Dots. *Nat. Biotechnol.* **2007**, *25*, 1165–1170.
 33. Li, S. D.; Huang, L. Pharmacokinetics and Biodistribution of Nanoparticles. *Mol. Pharm.* **2008**, *5*, 496–504.
 34. de Rosales, R. T. M.; Finucane, C.; Mather, S. J.; Blower, P. J. Bifunctional Bisphosphonate Complexes for the Diagnosis and Therapy of Bone Metastases. *Chem. Commun.* **2009**, 4847–4849.
 35. Benyettou, F.; Lalatonne, Y.; Sainte-Catherine, O.; Monteil, M.; Motte, L. Superparamagnetic Nanovector with Anti-cancer Properties: Gamma Fe₂O₃@Zoledronate. *Int. J. Pharm.* **2009**, *379*, 324–7.
 36. Clearfield, A. Recent Advances in Metal Phosphonate Chemistry II. *Curr. Opin. Solid State Mater. Sci.* **2002**, *6*, 495–506.
 37. Gao, W.; Dickinson, L.; Grozinger, C.; Morin, F. G.; Reven, L. Self-Assembled Monolayers of Alkylphosphonic Acids on Metal Oxides. *Langmuir* **1996**, *12*, 6429–6435.
 38. Lalatonne, Y.; Paris, C.; Serfaty, J. M.; Weinmann, P.; Lecouvey, M.; Motte, L. Bis-phosphonates-Ultra Small Superparamagnetic Iron Oxide Nanoparticles: A Platform Towards Diagnosis and Therapy. *Chem. Commun.* **2008**, 2553–5.
 39. Mohapatra, S.; Pramanik, P. Synthesis and Stability of Functionalized Iron Oxide Nanoparticles Using Organophosphorus Coupling Agents. *Colloids Surf., A: Physico-chem. Eng. Aspects* **2009**, *339*, 35–42.
 40. Portet, D.; Denizot, B.; Rump, E.; Lejeune, J. J.; Jallet, P. Nonpolymeric Coatings of Iron Oxide Colloids for Biological Use as Magnetic Resonance Imaging Contrast Agents. *J. Colloid Interface Sci.* **2001**, *238*, 37–42.
 41. Rutledge, R. D.; Warner, C. L.; Pittman, J. W.; Addleman, R. S.; Engelhard, M.; Chouyyok, W.; Warner, M. G. Thiol-Ene Induced Diphosphonic Acid Functionalization of Superparamagnetic Iron Oxide Nanoparticles. *Langmuir* **2010**, *26*, 12285–12292.
 42. Sahoo, Y.; Pizem, H.; Fried, T.; Golodnitsky, D.; Burstein, L.; Sukenik, C. N.; Markovich, G. Alkyl Phosphonate/Phosphate Coating on Magnetite Nanoparticles: A Comparison with Fatty Acids. *Langmuir* **2001**, *17*, 7907–7911.
 43. Ali, Z.; Abbasi, A. Z.; Zhang, F.; Arosio, P.; Lascialfari, A.; Casula, M. F.; Wenk, A.; Kreyling, W.; Plapper, R.; Seidel, M.; et al. Multifunctional Nanoparticles for Dual Imaging. *Anal. Chem.* **2011**, *83*, 2877–2882.
 44. Gehrke, N.; Briel, A.; Ludwig, F.; Remmer, H.; Wawrzik, T.; Wellert, S. New Perspectives for MPI: A Toolbox for Tracer Research Magnetic Particle Imaging. In *Magnetic Particle Imaging*, Buzug, T. M.; Borgert, J., Eds.; Springer: Berlin Heidelberg, 2012; Vol. 140, pp 99–103.
 45. Gossuin, Y.; Gillis, P.; Hocq, A.; Vuong, Q. L.; Roch, A. Magnetic Resonance Relaxation Properties of Superparamagnetic Particles. *Wires Nanomed. Nanobiol.* **2009**, *1*, 299–310.
 46. Simon, G. H.; Bauer, J.; Saborovski, O.; Fu, Y. J.; Corot, C.; Wendland, M. F.; Daldrup-Link, H. E. T1 and T2 Relaxivity of Intracellular and Extracellular USPIO at 1.5T and 3T Clinical MR Scanning. *Eur. Radiol.* **2006**, *16*, 738–745.
 47. Xiao, L.; Li, J.; Brougham, D. F.; Fox, E. K.; Feliu, N.; Bushmelev, A.; Schmidt, A.; Mertens, N.; Kiessling, F.; Valdor, M.; et al. Water-Soluble Superparamagnetic Magnetite Nanoparticles with Biocompatible Coating for Enhanced Magnetic Resonance Imaging. *ACS Nano* **2011**, *5*, 6315–6324.
 48. Casula, M. F.; Floris, P.; Innocenti, C.; Lascialfari, A.; Marinone, M.; Corti, M.; Sperling, R. A.; Parak, W. J.; Sangregorio, C. Magnetic Resonance Imaging Contrast Agents Based on Iron Oxide Superparamagnetic Ferrofluids. *Chem. Mater.* **2010**, *22*, 1739–1748.
 49. Weissleder, R.; Elizondo, G.; Wittenberg, J.; Rabito, C. A.; Bengele, H. H.; Josephson, L. Ultrasmall Superparamagnetic Iron-Oxide—Characterization of a New Class of Contrast Agents for MR Imaging. *Radiology* **1990**, *175*, 489–493.
 50. Hu, F. Q.; Jia, Q. J.; Li, Y. L.; Gao, M. Y. Facile Synthesis of Ultrasmall PEGylated Iron Oxide Nanoparticles for Dual-contrast T-1- and T-2-weighted Magnetic Resonance Imaging. *Nanotechnology* **2011**, *22*.
 51. Reiser, M.; Semmler, W.; Hricak, H. *Magnetic Resonance Tomography*; Springer: Berlin, 2008; p xxvii, 1511 p.
 52. Lodhia, J.; Mandarano, G.; Ferris, N. J.; Eu, P.; Cowell, S. F. Development and Use of Iron Oxide Nanoparticles (Part 1): Synthesis of Iron Oxide Nanoparticles for MRI. *Biomed. Imaging Intervention J.* **2010**, *6*, e12.
 53. Persigehl, T.; Bieker, R.; Matuszewski, L.; Wall, A.; Kessler, T.; Kooijman, H.; Meier, N.; Ebert, W.; Berdel, W. E.; Heindel, W.; et al. Antiangiogenic Tumor Treatment: Early Noninvasive Monitoring with USPIO-Enhanced MR Imaging in Mice. *Radiology* **2007**, *244*, 449–456.
 54. McRobbie, D. W., *MR from Picture to Proton*, 2nd ed.; Cambridge University Press: Cambridge, 2007.
 55. Li, W.; Tutton, S.; Vu, A. T.; Pierchala, L.; Li, B. S. Y.; Lewis, J. M.; Prasad, P. V.; Edelman, R. R. First-Pass Contrast-Enhanced Magnetic Resonance Angiography in Humans Using Ferumoxytol, a Novel Ultrasmall Superparamagnetic Iron Oxide (USPIO)-Based Blood Pool Agent. *J. Magn. Reson. Imaging* **2005**, *21*, 46–52.
 56. Allkemper, T.; Bremer, C.; Matuszewski, L.; Ebert, W.; Reimer, P. Contrast-Enhanced Blood-Pool MR Angiography with Optimized Iron Oxides: Effect of Size and Dose on Vascular Contrast Enhancement in Rabbits. *Radiology* **2002**, *223*, 432–438.
 57. Wagner, M.; Wagner, S.; Schnorr, J.; Schellenberger, E.; Kivelitz, D.; Krug, L.; Dewey, M.; Laule, M.; Hamm, B.; Taupitz, M. Coronary MR Angiography Using Citrate-Coated Very Small Superparamagnetic Iron Oxide Particles as Blood-Pool Contrast Agent: Initial Experience in Humans. *J. Magn. Reson. Imaging* **2011**, *34*, 816–823.
 58. Fretz, C. J.; Elizondo, G.; Weissleder, R.; Hahn, P. F.; Stark, D. D.; Ferrucci, J. T. Superparamagnetic Iron Oxide-Enhanced MR Imaging—Pulse Sequence Optimization for Detection of Liver-Cancer. *Radiology* **1989**, *172*, 393–397.
 59. Imaging of earlier time points could not be achieved due to the low radiochemical yields obtained.
 60. Keliher, E. J.; Yoo, J.; Nahrendorf, M.; Lewis, J. S.; Marinelli, B.; Newton, A.; Pittet, M. J.; Weissleder, R. Zr-89-Labeled Dextran Nanoparticles Allow *in Vivo* Macrophage Imaging. *Bioconjugate Chem.* **2011**, *22*, 2383–2389.
 61. Chao, Y.; Makale, M.; Karmali, P. P.; Sharikov, Y.; Tsigelny, I.; Merkulov, S.; Kesari, S.; Wrasidlo, W.; Ruoslahti, E.; Simberg, D. Recognition of Dextran-Superparamagnetic Iron Oxide Nanoparticle Conjugates (Feridex) via Macrophage Scavenger Receptor Charged Domains. *Bioconjugate Chem.* **2012**, *23*, 1003–1009.
 62. Miller, P. D. The Kidney and Bisphosphonates. *Bone* **2011**, *49*, 77–81.
 63. Makowski, M. R.; Wiethoff, A. J.; Blume, U.; Cuello, F.; Warley, A.; Jansen, C. H. P.; Nagel, E.; Razavi, R.; Onthank, D. C.; Cesati, R. R.; et al. Assessment of Atherosclerotic Plaque Burden with an Elastin-Specific Magnetic Resonance Contrast Agent. *Nat. Med.* **2011**, *17*, 383–388.